Constructive Quantum Interference in Photochemical Reactions

Sumit Suresh Kale, Yong P. Chen, and Sabre Kais*

Read Online

ACCESS | Metrics & More | Article Recommendations | SI Supporting Information

ABSTRACT: Interferences emerge when multiple pathways coexist together, leading toward the same result. Here, we report a theoretical study for a reaction scheme that leads to constructive quantum interference in a photoassociation (PA) reaction of a ^{87}Rb Bose−Einstein condensate where the reactant spin state is prepared in a coherent superposition of multiple bare spin states. This is achieved by changing the reactive scattering channel in the PA reaction. As the origin of coherent control comes from the spin part of the wavefunction, we show that it is sufficient to use radio frequency (RF) coupling to achieve the superposition state. We simulate the RF coupling on a quantum processor (IBMQ Lima), and our results show that interferences can be used as a resource for the coherent control of photochemical reactions. The approach is general and can be employed to study a wide spectrum of chemical reactions in the ultracold regime.
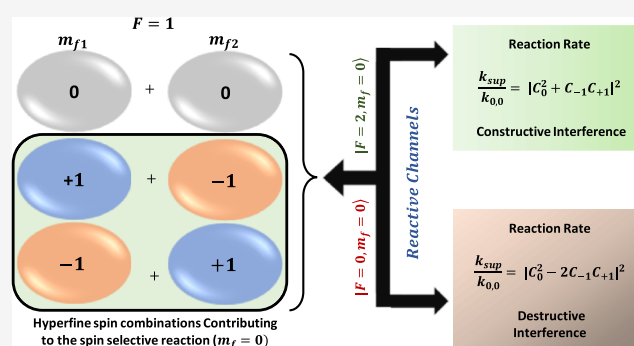
Observation of quantum interference is a common phenomenon in the physics of elastic collisions, but when it comes to inelastic collisions (many chemical reactions), it is quite rare. Several experiments[1−3] have shown that if there exist multiple pathways for a chemical reaction, then these pathways may interfere with each other producing interference patterns. In a recent study, Hu et al.[4] coherently controlled an ultracold chemical reaction by employing nuclear spin conservation during the experiment, which provides unprecedented quantum-state control over the reactants and products in a chemical reaction of two KRb molecules. In another study, Devolder et al.[5] developed a novel theory that uses quantum interference for complete coherent control in the ultracold regime where a single partial wave is dominant. This is achieved by changing the populations and the relative phases of the initial coherent superposition of degenerate molecular states. The theory showed an ultimate coherent control over ultracold spin-exchange collisions of oxygen molecules. An experimentally feasible quantum-interference-based approach has been shown theoretically[6] which extracts features from the differential cross-section for the coherent control in reactive collisions at low temperatures.

Blasing et al.[7] carried out an experiment that tried to answer the question "what happens in the reaction when the reactants are prepared in a quantum superposition?" The result was complete suppression of the chemical reaction which is explained by the destructive interference between different reaction pathways. In this theoretical study, we will show how can we achieve constructive interference by changing the reactive scattering channel. In addition, we explain how superposition is achieved in the reactants using Raman

coupling and radio frequency (RF) coupling. Finally, our study generalizes the findings by Blasing et al.[7] to constructive interference.

Photoassociation (PA)[8] is a light-aided chemical process where two atoms absorb a photon producing a bounded excited molecule while scattering. When we operate PA in the ultracold regime, it involves only a small number of scattering channels. Experimentally, a Bose Einstein condensate (BEC) of ^{87}Rb can be prepared in a $f = 1$ hyperfine state via optical evaporation.[9] The magnetic field tuning during the optical evaporation results in a BEC with bare $m_f = -1$, 0, +1 spin states or a statistical mixture of all three. In our calculations, we consider a BEC of ^{87}Rb in $f = 1$ and $m_f = 0$ bare spin states.

USING RAMAN COUPLING TO ACHIEVE SUPERPOSITION

A superposition state can be experimentally achieved by applying two counter-propagating Raman lasers adiabatically which drives transitions between these atomic Zeeman levels.[10,11] As a result, the Rb atom makes a transition from m_f to an $m_f - 1$ hyperfine Zeeman state by absorbing and emitting a photon. This process induces, in addition, a change in the momentum of the atom by $2k_r$, where k_r is the photon recoil momentum.[12,13] Thus, the atoms are dressed into a

superposition of hyperfine spin and mechanical momenta. In our previous work,[14] we analyzed the spin−orbit coupling in the BECs that realize a pair of qutrits. The Hamiltonian[12,13] that describes such a spin (m_f)—momentum (K) coupling can be written in the coupled basis $|m_f, K\rangle = \{|-1, q + 2K_r\rangle, |0, q\rangle, |+1, q - 2k_r\rangle\}$ as

$$H_0 = \begin{pmatrix} \frac{\hbar^2}{2m}(q + 2k_r)^2 & \frac{\Omega_r}{2} & 0 \\ -\delta(B) & & \\ \frac{\Omega_r}{2} & \frac{\hbar^2}{2m}q^2 - \epsilon(B) & \frac{\Omega_r}{2} \\ 0 & \frac{\Omega_r}{2} & \frac{\hbar^2}{2m}(q - 2k_r)^2 \\ & & + \delta(B) \end{pmatrix}$$

(1)

Here, m is the mass of ^{87}Rb, q is the quasi-momentum (usually at the minimum of the BEC's lowest energy band), Ω_r is the strength of the Raman coupling (which determines the Rabi frequency for the Raman transition between two hyperfine m_f states), $\delta(B)$ is the detuning of the Raman laser, $\epsilon(B) = 0.65E_r$ is the quadratic Zeeman shift (at $|B_{bias}| \approx 5G$), $E_r = \hbar k_r^2/2m$ is the recoil energy, and B is the strength of the external magnetic field. In deriving Hamiltonian (1), we made use of the rotating-wave approximation. After applying the Raman lasers, the population is transferred to $m_f = 1$ and $m_f = -1$ from an initially created $m_f = 0$ state due to which the BEC eventually ends up in the ground state of Hamiltonian (1), described by

$$|\psi_0\rangle = C_{-1}|q + 2k_r, -1\rangle + C_0|q, 0\rangle + C_1|q - 2k_r, 1\rangle$$

(2)

Here, $C_{\pm 1}$ and C_0 are coefficients of the superposition ground state as a result of coupling. The laser that drives a spin-sensitive PA transition is then applied in the experiment, selectively photoassociating only those colliding atoms (denoted as a and b here) whose total angular momentum $|F = f_a + f_b, m_f = m_{f,a} + m_{f,b}\rangle = |0, 0\rangle$. Using the single particle basis, $|f_a, m_{f,a}\rangle|f_b, m_{f,b}\rangle$,

$$|F = 0, m_f = 0\rangle = (|1, -1\rangle|1, +1\rangle - |1, 0\rangle|1, 0\rangle + |1, +1\rangle|1, -1\rangle)/\sqrt{3}$$

After considering the indistinguishable nature of bosons, we see that there are two pathways for this transition. Bosons with $m_f = \mp 1$ and $m_f = \pm 1$ combine together to give a molecule in $m_f = 0$, and similarly two individual Bosons in $m_f = 0$ do the same job. Therefore, the PA reaction happens through two pathways simultaneously. Both the reaction pathways contribute toward the total reaction rate with opposite signs due to opposite Clebsch−Gordon (CG) coefficients ($\pm 1/\sqrt{3}$ for $|F = 0, m_f = 0\rangle$), and the contribution also depends on the coefficients of the superpositioned states from eq 2. The rate of the PA reaction $k_{PA} \propto |\langle\psi_{mol}|\vec{d}\cdot\vec{E}|\psi_{scat}\rangle|^2$, where the proportionality factor is independent of the spin,[15] ψ_{mol} and ψ_{scat} are the total molecular and scattering wavefunctions. $\vec{E}$ and $\vec{d}$ correspond to the electric field of the PA laser and the dipole operator. For the Raman dressed atoms in the $|F = 0, m_f = 0\rangle$ scattering channel, the ratio of reaction rates between atoms in the superposition (k_{sup}) and bare spin ($k_{0,0}$) states is[7,16,17]

$$\frac{k_{sup}}{k_{0,0}} = |C_0^2|^2 + 4|C_{-1}C_1|^2 - 4\text{Re}[C_0^2 C_{-1}^* C_1^*]$$

(3)

The last term becomes negative because of the opposite sign of CG coefficients. $\Omega_r = 0$ and $\delta = 0$ can be visualized as not applying the Raman coupling beams, and thus, we no longer have the superposition in the reactant. This corresponds to all the population of BEC in the $|f = 1, m_f = 0\rangle$ hyperfine state ($C_0 = 1$, $C_{\pm 1} = 0$ in eq 3) and thus $k_{sup}/k_{0,0} \rightarrow 1$. At large values of Raman coupling and zero detuning, half of the population is transferred equally to $|f = 1, m_f = 1\rangle$ and $|f = 1, m_f = -1\rangle$ from $|f = 1, m_f = 0\rangle$ hyperfine spin state, which results in the convergence of the coefficients of the ground state $C_{\pm 1} \rightarrow 1/2$ and $C_0 \rightarrow 1/\sqrt{2}$, resulting in the reaction rate ratio (eq 3) $k_{sup}/k_{0,0} \rightarrow 0$ (destructive interference).

Now consider what happens if we change the reaction scheme and use a PA reaction which selectively photoassociates only those colliding atoms (denoted as a and b here) whose total angular momentum $|F = f_a + f_b, m_f = m_{f,a} + m_{f,b}\rangle = |2, 0\rangle$. Using the single particle basis, $|f_a, m_{f,a}\rangle|f_b, m_{f,b}\rangle$,

$$|F = 2, m_f = 0\rangle = (|1, -1\rangle|1, +1\rangle + 2|1, 0\rangle|1, 0\rangle + |1, +1\rangle|1, -1\rangle)/\sqrt{6}$$

The detailed theoretical discussion of the reaction rate ratio calculation for this scheme is available in the Supporting Information. The ratio of reaction rates for this reaction scheme is

$$\frac{k_{sup}}{k_{0,0}} = |C_0^2|^2 + |C_1 C_{-1}|^2 + 2\text{Re}[C_0^2 C_1^* C_{-1}^*]$$

(4)

Here, we see that due to same signs of the CG coefficients for the scattering channel $|F = 2, m_F = 0\rangle$ the last term comes out to be positive, and this increment is solely caused by the constructive interference between the reactive channels.

Figure 1a shows the normalized PA rate ratio $k_{sup}/k_{0,0}$ of BEC for the $|F = 0, m_f = 0\rangle$ channel, as a function of Raman coupling Ω_r/E_r which ranges from 0 to 15 at detuning $\delta = 0E_r$. We see that when $\Omega_r/E_r = 0$ which is equivalent to no Raman beam being applied, and as a result, we do not have any superposition in the reactant state, $C_0 = 1$ and $C_{\pm 1} = 0$ in eq 3, thus $k_{sup}/k_{0,0} \rightarrow 1$. Superposition states induced by a large Raman coupling and zero Raman detuning, nearly complete suppression of the PA rate is observed (red curve), which is interpreted as destructive interference. Our result is consistent with the experiment[7] where a complete suppression of the PA reaction was observed although the PA laser remained on. Figure 1b corresponds to the $|F = 2, m_f = 0\rangle$ scattering channel, where we see that the reaction rate ratio for the case when we consider interference (blue curve) is always higher than the case without the interference term, which we interpret as constructive interference.

We next study the effect of detuning δ/E_r on the PA rate. Since the BEC is prepared at the band minima, first the dressed band structure was calculated for $\Omega_r = 5.4E_r$, and different values of δ/E_r and the quasi-momentum values were obtained (corresponding to the minimum energy for a particular δ value). These values were used in Hamiltonian 1 to obtain the superposition coefficients, and then, the reaction rate ratios were calculated. Figure 2 shows the normalized PA rate ratio $k_{sup}/k_{0,0}$ at different values of detuning δ/E_r ranging from −3 to 3 and at Raman coupling $\Omega_r = 5.4E_r$. Figure 2a shows the
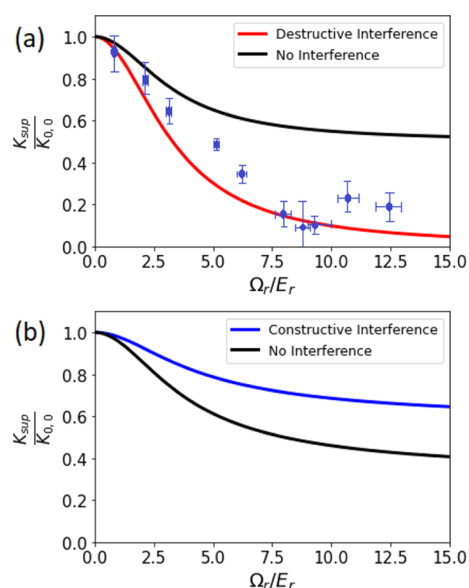
Figure 1. PA rate ratio $k_{sup}/k_{0,0}$ of BEC, as a function of Raman coupling Ω_r/E_r at detuning $\delta = 0E_r$, panel (a) shows the curve for the channel $|F = 0, m_f = 0\rangle$. The black (red) curve corresponds to theoretical prediction without (with) the destructive interference term in eq 3. The curve for the channel $|F = 2, m_f = 0\rangle$ is shown in panel (b). The black (blue) curve corresponds to theoretical prediction without (with) the constructive interference term in eq 4. The blue data points in (a) are the experimental data points from a study by Blasing et al.[7]
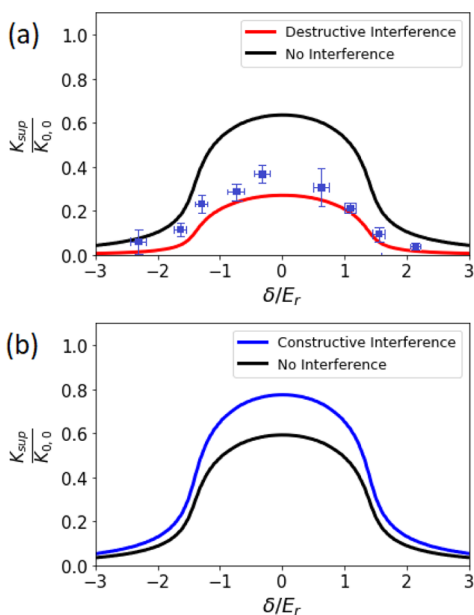

Figure 2. PA rate ratio $k_{sup}/k_{0,0}$ as a function of δ/E_r at $\Omega_r = 5.4E_r$, panel (a) shows the curve for the channel $|F = 0, m_f = 0\rangle$. The black (red) curve corresponds to theoretical prediction without (with) the destructive interference term in eq 3. The curve for the channel $|F = 2, m_f = 0\rangle$ is shown in panel (b). The black (blue) curve corresponds to theoretical prediction without (with) the constructive interference term in eq 4. The blue data points in (a) are the experimental data points from Blasing et al.[7]

results corresponding to the $|F = 0, m_f = 0\rangle$ channel where we see that the reaction rate ratio is always lower when we consider the interference (red curve) denoting destructive

interference. Our result is consistent with experimental findings.[7] As shown in Figure 2b, our theory predicts that the reaction rate ratio should be always higher in the case when we consider interference (blue) as compared to the no-interference case (black curve) which denotes constructive interference. Additionally, it is worthwhile to note that the difference is highest between these two cases when the Raman beam is resonant (the detuning δ is 0 E_r). It happens because when the Raman beam is resonant, it results in more population transfer to $m_f = \pm 1$ from $m_f = 0$ (increase in $C_{\pm 1}$ and decrease in C_0 in 2), and as we increase the detuning $\approx \pm 2E_r$, the majority of population is transferred in either $m_f = \mp 1$ which suggests that $C_0 = 0$ and one of $C_\pm = 0$ which makes $k_{sup}/k_{0,0} \to 0$ (eqs 3 and 4).

■ USING RF TO ACHIEVE SUPERPOSITION

Since PA control only comes from the spin part of the superposition wavefunction, the momentum part created by the Raman beam is a distraction for the underlying Physics. Thus, it is sufficient to use RF to couple different m_f spin states which we model below. The three-level hyperfine spin states can be schematically represented by a pair of Bloch spheres,[18] where one pole corresponds to $m_f = 0$ and another pole corresponds to $m_f = \pm 1$. Initially created BEC of ^{87}Rb in $f = 1$ and $m_f = 0$ bare spin state is now coupled to the $m_f = \pm 1$ states with a RF field. By controlling the time for which the RF pulse is applied, we can introduce a rotation along $Y(\theta_y)$, as shown in Figure 3a. As a result of rotation, the population transfer takes place. We simulated the θ_y rotation via a state vector simulator in Qiskit[19] and confirmed the results by comparing it with the calculations obtained from the IBM quantum device. Figure 3b
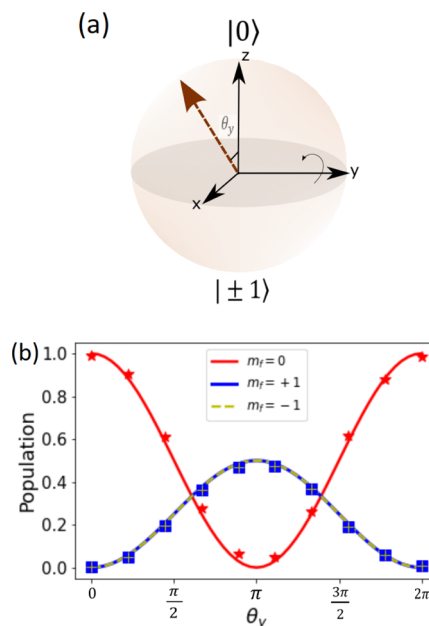

Figure 3. Achieving superposition using RF pulse, panel (a) shows the schematic representation of the rotation θ_y along the Y-axis on the Bloch sphere. Panel (b) shows the redistribution of the population as a function of θ_y. The red curve corresponds to state vector simulation of $m_f = 0$ population, and the asterisk data points on it corresponds to data obtained from the IBM quantum device. Similarly, the blue (yellow dash) curve corresponds to $m_f = +1(-1)$, and the square(plus) data points on it corresponds to data obtained from the IBM quantum device (IBMQ_Lima).

shows the population distribution as a function of θ_y. Initially (at $\theta_y = 0$), all the population exists only in the $m_f = 0$ state. As we increase θ_y, the population transfer initiates. At $\theta_y = \pi/2$, we see half of the population is in $m_f = 0$, and the remaining half is equally distributed in $m_f = \pm 1$. At $\theta_y = \pi$, the entire population is distributed equally in $m_f = \pm 1$ states. After this point, if we increase θ_y, the $m_f = 0$ population increases again and shows symmetric behavior ($\theta_y = \pi$ represents the south pole on a Bloch sphere, as shown in Figure 3a, and after this instant, further rotation will take the state vector toward the north pole making population symmetric about π). The population distribution, as shown in Figure 3b, goes well with the experimentally observed results in Figure 1D of ref 18 for the time scale of 40 μs.

As a result of RF coupling which results in population transfer to $m_f = 1$ and $m_f = -1$ from an initially created $m_f = 0$ state, the spin part of the scattered wavefunction for a single BEC eventually ends up in a superposition described by

$$|\phi_a'\rangle = C_{-1}'|1, -1\rangle_a + C_0'|1, 0\rangle_a + C_{+1}'|1, 1\rangle_a \qquad (5)$$

where $C_{-1}' = \sin(\theta_y/2)/\sqrt{2}$, $C_0' = \cos(\theta_y/2)$, and $C_{+1}' = \sin(\theta_y/2)/\sqrt{2}$ are the coefficients of superposition, the first and the second number inside the ket denote $F = 1$ and the associated hyperfine spin (m_f), respectively. Equation 5 shows that the superposition created via RF does not have any momentum parts and thus is much simpler to work with. The reaction rates ratios for both the reaction channels do not change, and eqs 3 and 4 still apply.

Figure 4a shows the normalized PA rate ratio $k_{sup}/k_{0,0}$ of BEC for the $|F = 0, m_f = 0\rangle$ channel, as a function of rotation
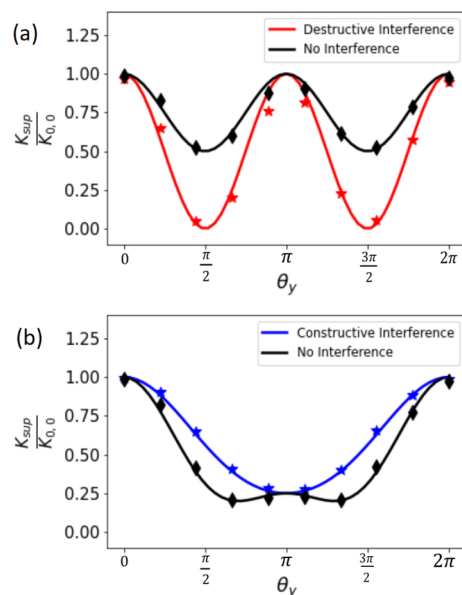

Figure 4. PA rate ratio $k_{sup}/k_{0,0}$ of BEC, as a function of θ_y, panel (a) shows the curve for the channel $|F = 0, m_f = 0\rangle$. The black (red) curve corresponds to theoretical prediction without (with) the destructive interference term in eq 3, and the black diamond (red asterisk) corresponds to data points obtained from the IBM device. The curve for the channel $|F = 2, m_f = 0\rangle$ is shown in panel (b). The black (blue) curve corresponds to theoretical prediction without (with) the constructive interference term in eq 4, and the black diamond(blue asterisk) corresponds to data points obtained from the IBM quantum device (IBMQ Lima).

along the Y-axis (θ_y) which ranges from 0 to 20. At $\theta_y = 0$, all the population exists in $m_f = 0$, and thus, we do not have superposition in the reactant state, which corresponds to $C_0' = 1$ and $C_{\pm 1}' = 0$ in eqs 5 and 3. Thus, $k_{sup}/k_{0,0} \rightarrow 1$. As we increase the angle of rotation θ_y, the population transfer takes place, as shown in Figure 3b, and the reaction rate ratio drastically falls down for the case in which we considered the interference (red curve/asterisks). At the rotation angle, $\theta_y = \pi/2$, the reaction is completely suppressed for the interference case. The reason being at this point half of the population is present in $m_f = 0$ state, and another half is equally distributed in $m_f = \pm 1$ states, which corresponds to $C_0' = 1/\sqrt{2}$ and $C_{\pm 1}' = 1/2$ in eq 3, leading to $k_{sup}/k_{0,0} \rightarrow 0$. At $\theta_y = \pi$, the reaction rate ratio for the interference case is $k_{sup}/k_{0,0} \rightarrow 1$, but the reason is entirely opposite to that of $\theta_y = 0$ case; at this point, all the population is equally distributed in $m_f = \pm 1$ states which corresponds to $C_0' = 0$ and $C_{\pm 1}' = 1/\sqrt{2}$. After this point, the trend repeats as expected from the population distribution. In general, the reaction rate ratio for the case where we consider interference (red curve) is always less (or equal as explained), compared to the case, in which we do not consider interference term (black cure) in eq 3, this is interpreted as destructive interference.

Similarly, Figure 4b shows the normalized PA rate ratio $k_{sup}/k_{0,0}$ of BEC for the $|F = 2, m_f = 0\rangle$ channel, as a function of rotation along the Y-axis (θ_y). At $\theta_y = 0$, $C_0' = 1$ and $C_{\pm 1}' = 0$, and this corresponds to $k_{sup}/k_{0,0} \rightarrow 1$ from eq 4. As we increase the angle of rotation θ_y, the population transfer takes place. At $\theta_y = \pi$, the reaction rate ratio for the case where we consider interference (blue curve) matches with the case where we do not consider interference. The reason being at this point all the population is equally distributed in $m_f = \pm 1$ which corresponds to $C_0' = 0$ and $C_{\pm 1}' = 1/\sqrt{2}$. Therefore, out of two reaction pathways, only one of them exists ($m_f = \pm 1 + m_f = \mp 1 \rightarrow m_{tot} = 0$). It is important to note that Figure 4a,b shows symmetry about $\theta_y = \pi$ which comes from the nature of population distribution, as shown in Figure 3b. Also, the periodicity of reaction rates, as shown in Figure 4a,b, is π and 2π, respectively. The origin of these periodicities can be explained via the symmetric nature of superposition coefficients along with the corresponding rate expressions (eqs 3 and 4). In general, the reaction rate ratio for the case where we consider interference (blue curve) is always greater (or equal as explained), compared to the case, in which we do not consider interference term (black cure) in eq 4, this is interpreted as constructive interference.

In summary, there are multiple approaches to achieve constructive interference within PA reaction. For example, the recent study by Kondakci et al.[18] showed the interferometric control over the $|F = 0, m_f = 0\rangle$ reaction channel by exploiting the quadratic Zeeman shift which introduces an additional relative phase between $m_f = 0$ and $m_f = \pm 1$ hyperfine spins in the superposition state eq 2. We have shown that by changing the scattering channel from $|F = 0, m_f = 0\rangle$ to $|F = 2, m_f = 0\rangle$, we can achieve a constructive interference. The reason behind this result is the similar (opposite) sign of CG coefficients in the latter (former). We are investigating the existence of a spin-sensitive PA frequency,[20] which corresponds to the $|F = 2, m_f = 0\rangle$ scattering channel. Our study shows that quantum interferences can be employed to coherently control a photochemical reaction. The approach is general and can be used to study a wide range of chemical reactions in the

ultracold regime. Next, we plan to investigate the role of entanglement[21−23] to control and predict the interference patterns observed in different scattering experiments which are similar to the PA reaction of SOC BEC.[3,24]

■ ASSOCIATED CONTENT

ⓢ Supporting Information

The Supporting Information is available free of charge at https://pubs.acs.org/doi/10.1021/acs.jctc.1c00826.

Detailed derivation of the reaction rate ratio calculations corresponding to the $|F = 2, m_f = 0\rangle$ reactive scattering channel (PDF)

■ AUTHOR INFORMATION

Corresponding Author

Sabre Kais − *Department of Chemistry, Department of Physics and Astronomy, and Purdue Quantum Science and Engineering Institute, Purdue University, West Lafayette, Indiana 47907, United States;* ⓞ orcid.org/0000-0003-0574-5346; Email: kais@purdue.edu

Authors

Sumit Suresh Kale − *Department of Chemistry, Purdue University, West Lafayette, Indiana 47907, United States;* ⓞ orcid.org/0000-0002-4537-1628

Yong P. Chen − *Department of Physics and Astronomy and Purdue Quantum Science and Engineering Institute, Purdue University, West Lafayette, Indiana 47907, United States*

Complete contact information is available at:
https://pubs.acs.org/10.1021/acs.jctc.1c00826

Notes

The authors declare no competing financial interest.

■ REFERENCES

(1) Jambrina, P. G.; Herráez-Aguilar, D.; Aoiz, F. J.; Sneha, M.; Jankunas, J.; Zare, R. N. Quantum interference between H+ D 2 quasiclassical reaction mechanisms. *Nat. Chem.* **2015**, *7*, 661.

(2) Dai, D.; Wang, C. C.; Harich, S. A.; Wang, X.; Yang, X.; Der Chao, S.; Skodje, R. T. Interference of quantized transition-state pathways in the H+ D2→ D+ HD chemical reaction. *Science* **2003**, *300*, 1730−1734.

(3) Sneha, M.; Gao, H.; Zare, R. N.; Jambrina, P. G.; Menéndez, M.; Aoiz, F. J. Multiple scattering mechanisms causing interference effects in the differential cross sections of H+D2→HD(v=4,j). *J. Chem. Phys.* **2016**, *145*, 024308.

(4) Hu, M.-G.; Liu, Y.; Nichols, M. A.; Zhu, L.; Quéméner, G.; Dulieu, O.; Ni, K.-K. Nuclear spin conservation enables state-to-state control of ultracold molecular reactions. *Nat. Chem.* **2021**, *13*, 435−440.

(5) Devolder, A.; Brumer, P.; Tscherbul, T. V. Complete quantum coherent control of ultracold molecular collisions. *Phys. Rev. Lett.* **2021**, *126*, 153403.

(6) Devolder, A.; Tscherbul, T.; Brumer, P. Coherent control of reactive scattering at low temperatures: Signatures of quantum interference in the differential cross sections for F+ H 2 and F+ HD. *Phys. Rev. A* **2020**, *102*, No. 031303(R).

(7) Blasing, D. B.; Pérez-Ríos, J.; Yan, Y.; Dutta, S.; Li, C. H.; Zhou, Q.; Chen, Y. P. Observation of quantum interference and coherent control in a photochemical reaction. *Phys. Rev. Lett.* **2018**, *121*, 073202.

(8) Jones, K. M.; Tiesinga, E.; Lett, P. D.; Julienne, P. S. Ultracold photoassociation spectroscopy: Long-range molecules and atomic scattering. *Rev. Mod. Phys.* **2006**, *78*, 483.

(9) Olson, A. J.; Niffenegger, R. J.; Chen, Y. P. Optimizing the efficiency of evaporative cooling in optical dipole traps. *Phys. Rev. A* **2013**, *87*, 053613.

(10) Lin, Y.-J.; Spielman, I. B. Synthetic gauge potentials for ultracold neutral atoms. *J. Phys. B: At., Mol. Opt. Phys.* **2016**, *49*, 183001.

(11) Spielman, I. B. *Annual Review of Cold Atoms and Molecules*; World Scientific, 2013; Vol. 1, pp 145−187.

(12) Lin, Y.-J.; Compton, R.; Perry, A.; Phillips, W.; Porto, J.; Spielman, I. Bose-Einstein condensate in a uniform light-induced vector potential. *Phys. Rev. Lett.* **2009**, *102*, 130401.

(13) Lin, Y.-J.; Jiménez-García, K.; Spielman, I. B. Spin−orbit-coupled Bose−Einstein condensates. *Nature* **2011**, *471*, 83−86.

(14) Kale, S. S.; Ding, Y.; Chen, Y. P.; Friedrich, B.; Kais, S. Spin-momentum entanglement in a Bose−Einstein condensate. *Phys. Chem. Chem. Phys.* **2020**, *22*, 25669−25674.

(15) Theis, M.; Thalhammer, G.; Winkler, K.; Hellwig, M.; Ruff, G.; Grimm, R.; Denschlag, J. H. Tuning the scattering length with an optically induced Feshbach resonance. *Phys. Rev. Lett.* **2004**, *93*, 123001.

(16) McKenzie, C.; et al. Photoassociation of Sodium in a Bose-Einstein Condensate. *Phys. Rev. Lett.* **2002**, *88*, 120403.

(17) Blasing, D. B.; Pérez-Ríos, J.; Yan, Y.; Dutta, S.; Li, C.-H.; Zhou, Q.; Chen, Y. P. Observation of Quantum Interference and Coherent Control in a Photochemical Reaction. *Phys. Rev. Lett.* **2018**, *121*, 073202.

(18) Kondakci, H. E.; Blasing, D. B.; Li, C.-H.; Chen, Y. P. Interferometric Control of Photo-Chemical Reactions in 87 Rb Bose-Einstein Condensates. *2020 Conference on Lasers and Electro-Optics (CLEO)*, 2020; pp 1−2.

(19) Abraham, H.; AduOffei; Agarwal, R.; Akhalwaya, I. Y.; Aleksandrowicz, G.; Alexander, T.; Čepulkovskis, M. *Qiskit: An Open-Source Framework for Quantum Computing*, 2019.

(20) Hamley, C. D.; Bookjans, E. M.; Behin-Aein, G.; Ahmadi, P.; Chapman, M. S. Photoassociation spectroscopy of a spin-1 Bose-Einstein condensate. *Phys. Rev. A* **2009**, *79*, 023401.

(21) Karra, M.; Sharma, K.; Friedrich, B.; Kais, S.; Herschbach, D. Prospects for quantum computing with an array of ultracold polar paramagnetic molecules. *J. Chem. Phys.* **2016**, *144*, 094301.

(22) Li, J.; Kais, S. Entanglement classifier in chemical reactions. *Sci. Adv.* **2019**, *5*, No. eaax5283.

(23) Kais, S. Entanglement, electron correlation, and density matrices. *Adv. Chem. Phys.* **2007**, *134*, 493.

(24) Liu, Y.; Hu, M.-G.; Nichols, M. A.; Yang, D.; Xie, D.; Guo, H.; Ni, K.-K. Precision test of statistical dynamics with state-to-state ultracold chemistry. *Nature* **2021**, *593*, 379−384.